ELSEVIER

Contents lists available at ScienceDirect

Chemical Engineering Journal

journal homepage: www.elsevier.com/locate/cej





Preparation of photo-crosslinked aliphatic polycarbonate coatings with predictable degradation behavior on magnesium-alloy stents by electrophoretic deposition

Kai Pan^a, Xiaojie Li^{a,*}, Hui Shi^a, Miao Dai^a, Zhenyu Yang^b, Maohua Chen^b, Wei Wei^a, Xiaoya Liu^{a,*}, Yufeng Zheng^c

- a Key Laboratory of Synthetic and Biological Colloids, Ministry of Education, School of Chemical and Material Engineering, Jiangnan University, Wuxi 214122, China
- b Department of Cardiology, The Affiliated Wuxi People's Hospital of Nanjing Medical University, Jiangsu Province, Wuxi 214023, China
- ^c State Key Laboratory for Turbulence and Complex Systems and Department of Materials Science and Engineering, College of Engineering, Peking University, Beijing 100871, China

ARTICLE INFO

Keywords:

Biodegradable aliphatic polycarbonate coating Magnesium alloy Cardiovascular stent Electrophoretic deposition

ABSTRACT

Magnesium-alloy stents (Mg-alloy stents), a new generation of bioabsorbable stents, are characterized by limited surface biocompatibility and premature loss of radial support due to rapid and inhomogeneous corrosion. While these disadvantages could be addressed by coating the stents with biodegradable polymeric material, most investigations have discussed the coating materials and coating technology separately without attempting to study their combined effect. Since Mg-alloy stents possess a complex mesh tube structure, the facile preparation of high-performance polymeric coatings without defects to control the excessive and inhomogeneous corrosion remains challenging. In this paper, we report the fabrication of aliphatic polycarbonate (APC) coatings by electrophoretic deposition (EPD) and subsequent photo-crosslinking to achieve corrosion resistance and surface biocompatibility enhancement of Mg-alloy stents. The EPD method enabled the facile preparation of APC coatings with a uniform surface, controllable thickness, and enhanced adhesion on AZ31 Mg stents. The photocrosslinking further enhanced the mechanical properties and durability of the coatings. The prepared APC coating demonstrated a predictable surface-erosion behavior, resulting in homogeneous and slow corrosion of AZ31 Mg alloy both in vitro and in vivo. The APC coating could not only effectively promote the adhesion and proliferation of endothelial cells but also improve the hemocompatibility and histocompatibility of Mg alloy. This study may offer a feasible and promising strategy for maintaining mechanical integrity and enhancing surface biocompatibility of Mg-alloy stents and other Mg-alloy implants.

1. Introduction

A cardiovascular stent consists of a small mesh tube and is used in the treatment of coronary artery diseases as a reliable device, which is implanted to reopen the occluded arteries after expansion [1]. Traditional permanent stents (including bare-metal stents and drug-eluting stents, made of stainless steel, titanium alloys, etc.) will elicit foreign body reactions [2] throughout a patient's lifetime, which results in chronic inflammation [3], in-stent restenosis [4], and late thrombosis [5]. In the last two decades, a new generation of biodegradable stents has emerged, which are expected to provide the initial necessary mechanical strength while spontaneously degrading and being absorbed

along with the vascular repair process [6]. This revolutionary stent has the potential to eliminate the mentioned weakness posed by permanent stents [7]. Magnesium (Mg) alloys have been considered a promising material for biodegradable stents [5,8] due to their biodegradability, favorable biocompatibility, and superior mechanical property [9,10]. As an essential substance for the human body, a Mg element intake of 240–400 mg/day is recommended for adults, and excessive Mg-cations, Mg²⁺, can be excreted through kidneys [11,12]. However, since Mg is a highly reactive metal (electrochemical potential of –2.37 V vs. SHE) [13], most Mg alloys possess a fast corrosion rate accompanied by the local release of excessive toxic ions and hydrogen gas (H₂) [14,15]. In addition, Mg alloys exhibit inhomogeneous corrosion behavior due to

E-mail addresses: xjli@jiangnan.edu.cn (X. Li), lxy@jiangnan.edu.cn (X. Liu).

^{*} Corresponding authors.

the pitting corrosion that easily occurs in physiological environments containing chloride ions [16]. The rapid and inhomogeneous degradation behavior of an implanted Mg-alloy stent would lead to local toxicity, tissue damage, and especially the premature loss of mechanical scaffolding support before full vascular repair [17,18]. Therefore, the realization of a slow and homogeneous degradation of Mg alloys is still a challenge for their application as stent material [19].

Although a few Mg alloys exhibit a relatively slow degradation rate dependent on their alloy design [20,21], biodegradable polymeric coating has been demonstrated as a more versatile approach to control the corrosion behavior and improve surface biocompatibility for Mgalloy implants, due to the good biocompatibility, design versatility, cost-effectiveness, and ease of process [22]. Earlier studies rarely considered the degradation behavior of polymeric coatings, although it directly influences the corrosion behavior of Mg substrates. For instance, many reports indicated that commercially available polyesters, such as poly(lactide-co-glycolic acid) (PLGA) and poly(L-lactic acid) (PLLA), effectively enhanced the corrosion resistance of Mg-alloy implants [23,24], and they also have been used as polymeric coatings on commercial Mg-alloy drug-eluting stents [5,25]. However, after long-term soaking in physiological media, polyester coatings are easily ruptured and exfoliated due to their bulk-eroding property [26] and unsatisfactory adhesion [27]. Furthermore, the acidic degradation products of polyesters easily cause inflammation of surrounding tissues [28]. In contrast, biodegradable aliphatic polycarbonates (APCs), especially poly (trimethylene carbonate) (PTMC) and its derivatives, could be coating candidates for Mg implants as they present as a unique surface-erosion behavior the degradation from surface to the interior, which can provide sufficient protection of the Mg implants from the corrosive media until their full biodegradation [29]. In addition, PTMC has been approved by the US Food and Drug Administration (FDA) and forms neutral degradation products which reduced the inflammatory tissue response [30]. Considering the mentioned advantages, APCs are almost tailored coating materials for Mg-alloy stents. The inhomogeneous and fast corrosion behavior of Mg alloys can be controlled both in vitro and in vivo by PTMC coating, and the corresponding surface bioactivity of Mgalloy implants was simultaneously improved [31]. In our previous study, we crosslinked PTMC-based coatings via photo-induced "thiol-ene" reaction, which improved the inherent PTMC drawbacks of poor mechanical stability and adhesion strength and resulted in a slower in vitro erosion rate (2-3 µm per month after crosslinking) [32]. Moreover, compared to the traditional photo-induced free radical polymerization, the photo-crosslinked networks formed by the thiol-ene reaction could be fully degraded, absence of potential non-degradable polymer crosslinks [33]. Therefore, the thiol-ene-crosslinked APC with predictable degradation behavior may be a promising coating material for Mg-alloy stents. Unfortunately, the tiny and complex mesh tube structure poses a considerable challenge for constructing smooth, uniform, thicknesscontrollable, and defect-free polymeric coatings on Mg-alloy stents by conventional coating methods such as dipping, spraying, and layer-bylayer assembly. Therefore, besides the coating materials, the coating method is another major factor for surface modification of Mg-alloy stents with an important contribution to coating efficacy.

In this work, we attempt to address the mentioned challenges by combining APC coating materials with electrophoretic deposition (EPD) coating strategy. EPD is a well-established coating preparation technique [34], in which charged colloidal particles move toward an oppositely charged electrode under a DC electric field and deposit on the electrode material and eventually form a coating by particles accumulation [35]. The quality and thickness of the deposited coating can be simply adjusted by the applied voltage, deposition time, and concentration of colloidal particles [36]. The EPD method includes the advantages of short operation time, use of simple apparatus, fine-tunable coating thickness, and the possibility of uniform deposition on substrate of complex geometries [37–40]. Many researches have used naturally occurring macromolecules to fabricate biocompatible coatings on Mg-

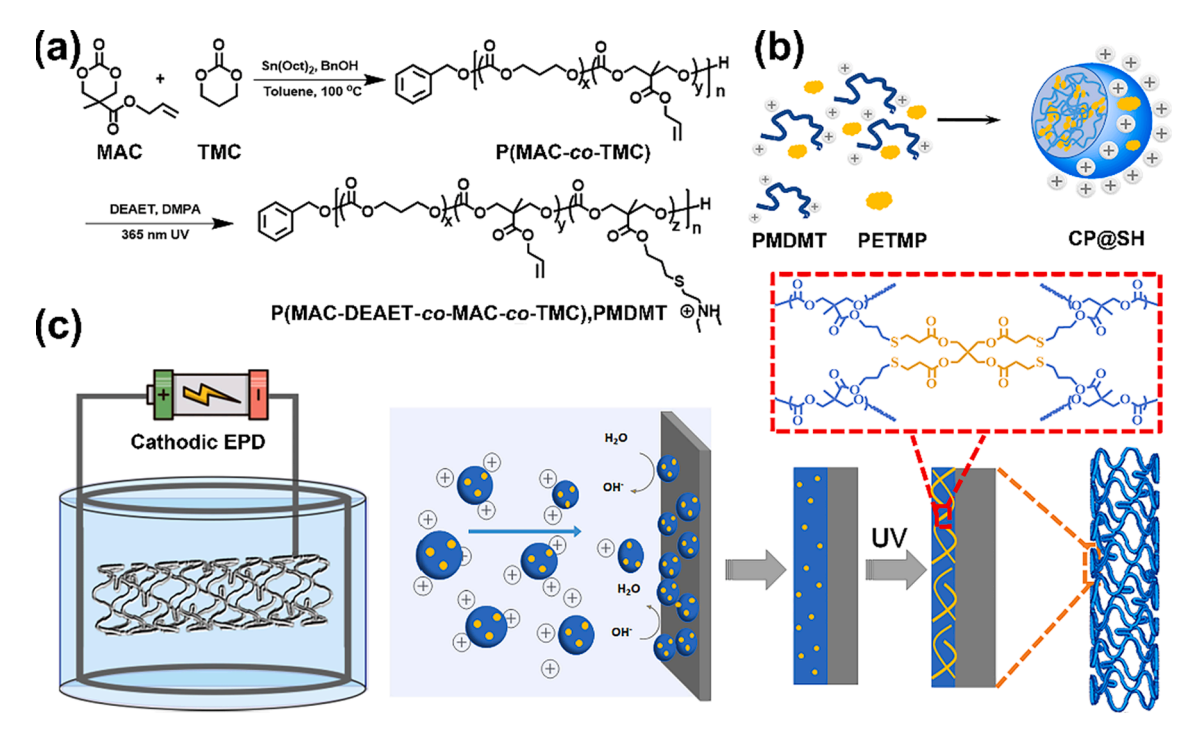
alloy stents by the EPD method [41–44]. However, their hydrophilic properties limited the corrosion resistance performance. We believe that the combination of surface-eroding APC materials and EPD coating technology will result in tailor-made biodegradable coating with excellent corrosion resistance to effectively control the excessive and inhomogeneous degradation of Mg-alloy stents. To verify our hypothesis, we prepared a thiol-ene photo-crosslinked APC coating by the EPD method on AZ31 Mg stents (Scheme 1). First, the cationic polycarbonate P(MAC-DEAET-co-MAC-co-TMC) (PMDMT) was synthesized by postpolymerization modification. Afterward, colloidal PMDMT particles pentaerythritol loaded with the crosslinker tetrakis(3mercaptopropionate) (PETMP) were obtained by a macromolecular self-assembly method. Finally, the colloidal particles were deposited on AZ31 Mg substrates (including sheets and stents) by cathodic EPD, and the crosslinked APC networks were formed after UV irradiation. The thickness control, adhesion strength, and surface morphologies of the EPD coating method were systematically evaluated for the modification of AZ31 Mg stents. The in vitro and in vivo corrosion behavior of the coated Mg samples was examined, and the anti-corrosion mechanism of the coating was discussed. The blood compatibility, in vitro endothelial cell adhesion and proliferation, and in situ inflammation behavior were assessed.

2. Results and discussion

2.1. Fabrication and characterization of photo-crosslinked polycarbonate EPD coatings

The degradable cationic polycarbonate PMDMT was first synthesized and characterized by ¹H NMR spectroscopy and DMF gel permeation chromatography (GPC) (Fig. S1, see supporting information). PETMP was then loaded on the PMDMT colloidal particles by a self-assembly method to afford CP@SH (Scheme 1b, Fig. S2), and colloidal particles (CP) without PMDMT were also prepared as a control. Since both CP@SH and CP possessed positive surface charge, they can be deposited on the Mg substrate of the cathode in a DC electric field. The coating thickness can be controlled by adjusting the concentration of colloidal particles, deposition time, and EPD voltage. To avoid too thick coating blocking the tiny bending parts of the Mg-alloy stent, the optimal EPD conditions were determined (Fig. S3) to produce coatings with a thickness of about 10 μm for further study (Fig. 1a). The chemical composition of photo-crosslinked CP@SH coating on AZ31 Mg (Mg-CP@SH) was assessed by attenuated total reflection Fourier-transform infrared spectroscopy (ATR-FTIR, Fig. 1b) and X-ray photoelectron spectroscopy (XPS, Fig. 1c). After modification by EPD coating, the Mg 2 s peak of the AZ31 Mg substrate was absent, and new peaks related to S 2 s and S 2p were observed. The quantitative sulfur content analysis results (Table S1) indicated that PETMP crosslinker was encapsulated in the colloidal particles and electrodeposited on the Mg substrate. The formation of photo-crosslinked networks in the CP@SH coating was examined by ATR-FTIR (Fig. 1b). The disappearance of the characteristic peak at 1646 cm⁻¹ (allyl group) and the intensity decrease of the absorption peak at 2560 cm⁻¹ (thiol group) after UV treatment indicated the presence of thiol-ene crosslinking.

The inadequate adhesion between polymeric coatings and Mg substrate is an inherent drawback and impedes the corrosion protection of coatings to a large extent. Hence, the adhesive strength of EPD coatings was measured (Fig. 1d). To discuss the effect of the coating method on adhesive strength, a coating prepared by the dip-coating method with the same crosslinked APC structure as the CP@SH coating was used for comparison (named PMDMT@SH coating). In comparison with the CP coating, a significant increase of adhesive strength was observed in both CP@SH and PMDMT@SH coating. The polar sulfide groups could enhance the interaction between the coating and Mg substrate, and the crosslinking improves the cohesive force of the coating material. As expect, the Mg-CP@SH sample presented better adhesive strength than



Scheme 1. Schematic illustration of stepwise fabrication of thiol-ene photo-crosslinked APC coating on AZ31 Mg stent by the EPD method: (a) synthetic route of the cationic polycarbonate P(MAC-DEAET-co-MAC-co-TMC) (PMDMT), (b) the preparation of CP@SH colloidal particles, and (c) electrodeposition of CP@SH colloidal particles on a Mg-alloy stent and photo-crosslinking via UV irradiation.

the PMDMT@SH coating, which may be attributed to an inherent adhesion advantage of the EPD method for coating materials [37].

Compared to PMDMT@SH-coated stent, the CP@SH-coated stent showed uniform and smooth surface morphologies (Fig. S4), indicating that EDP was an efficient coating technology for metallic stents with complex structure. During the surgical implantation, sufficient adhesion and flexibility of the Mg-alloy stent coatings are very important because the stents undergo severe deformation during balloon expansion. Once the coating cracks due to the concentrated stress during expansion, the protection by the coating will be lost and the Mg substrate will be attacked by the surrounding physiological medium. To assess the performance under such practical conditions, the adhesion and flexibility of the CP@SH coating were evaluated by balloon expansion tests (Fig. S5), and the morphology of the AZ31 Mg stents was examined by SEM (Fig. 1e) especially in the bend area of the CP@SH-coated stent where the stress is most concentrated [45]. After expansion, no signs of peeling and spallation of the CP@SH coating from the Mg-alloy stent were observed. In addition, as shown in high magnification SEM images of the bend area, no microcracks were observed on the expanded surface indicating excellent adhesion and flexibility of CP@SH coating. The superior flexibility may be attributed to the formation of a soft, crosslinked, APC network. In summary, the thiol-ene-crosslinked APC coating exhibits a controllable thickness, uniform distribution, excellent flexibility, and outstanding adhesion because of the combination of a versatile EPD method and favorable coating material, which constitutes a promising strategy for the design of Mg-alloy stent coatings.

2.2. Electrochemical test

The corrosion rate and behavior of different samples were analyzed by an electrochemical assessment method in simulated body fluid (SBF). The presence of coating increased corrosion potential ($E_{\rm corr}$) and reduced corrosion current density ($I_{\rm corr}$) of the Mg substrate (Fig. 2 a-b). Specifically, the $E_{\rm corr}$ (vs. SCE) of -1.70 V of the bare AZ31 increased to -1.55 and -1.49 V for Mg-CP and Mg-CP@SH, respectively. The $I_{\rm corr}$ values of the bare AZ31, Mg-CP, and Mg-CP@SH were determined as

 1.53×10^{-3} , 3.59×10^{-5} , and 4.85×10^{-6} A/cm², respectively. The results suggested that polycarbonate coatings generated by EPD protect Mg alloy effectively from rapid corrosion at the early stage of immersion. Due to the formation of cross-links, the anti-corrosion properties of the Mg-CP@SH sample were further enhanced, which was confirmed by the polarization resistance (R_p) increase from 727.23 Ω cm² (Mg-CP) to 4204.8 Ω cm² (Mg-CP@SH). To visually evaluate the protective effect, the corrosion rate (CR), calculated based on their corresponding I_{corr} , was used to describe the corrosion rate of different samples. The Mg-CP@SH sample exhibited a fairly low corrosion rate (0.11 mm/year), which was not only lower than that of the Mg-CP sample (0.80 mm/ year) but also two orders of magnitude lower than that of AZ31 (34.20 mm/year). Therefore, one can conclude from these results that polymer coatings truly enhance the corrosion resistance of Mg alloy due to the isolation of Mg substrates from corrosive media; the formation of photocrosslinked polycarbonate networks further improves the isolation performance, resulting in a large deceleration of the corrosion rate of the Mg substrate.

To compare and evaluate the corrosion resistance of polymer coatings, the corrosion characteristics of different samples were investigated by electrochemical impedance spectroscopy (EIS) (Fig. 2c-e). In general, a larger diameter of the capacitive loop, higher |Z| modulus at 10^{-2} Hz (the lowest test frequency), and higher phase angle indicate better corrosion resistance of Mg substrates. Compared to bare Mg (Fig. S6), the capacitive loop attributed to the charge transfer process dramatically increased after coating modification (Fig. 2c), indicating the enhancement of corrosion resistance. The inductive loops of both bare Mg and Mg-CP samples were related to the dissolution and pitting corrosion of Mg substrate [46]. The results indicated that, although the application of CP coating clearly increased the protection performance of Mg substrate, it failed to prevent Mg dissolution. The inductive loop was absent on the Nyquist plot of Mg-CP@SH, which indicated that CP@SH completely inhibited the penetration of corrosive media, probably due to the effective improvement of its stability and its function as a barrier after the formation of polycarbonate networks. The |Z| value of Mg-CP@SH $(2.94 \times 10^5~\Omega~cm^2)$ was far higher than that of Mg-CP $(1.21 \times 10^4~\Omega$

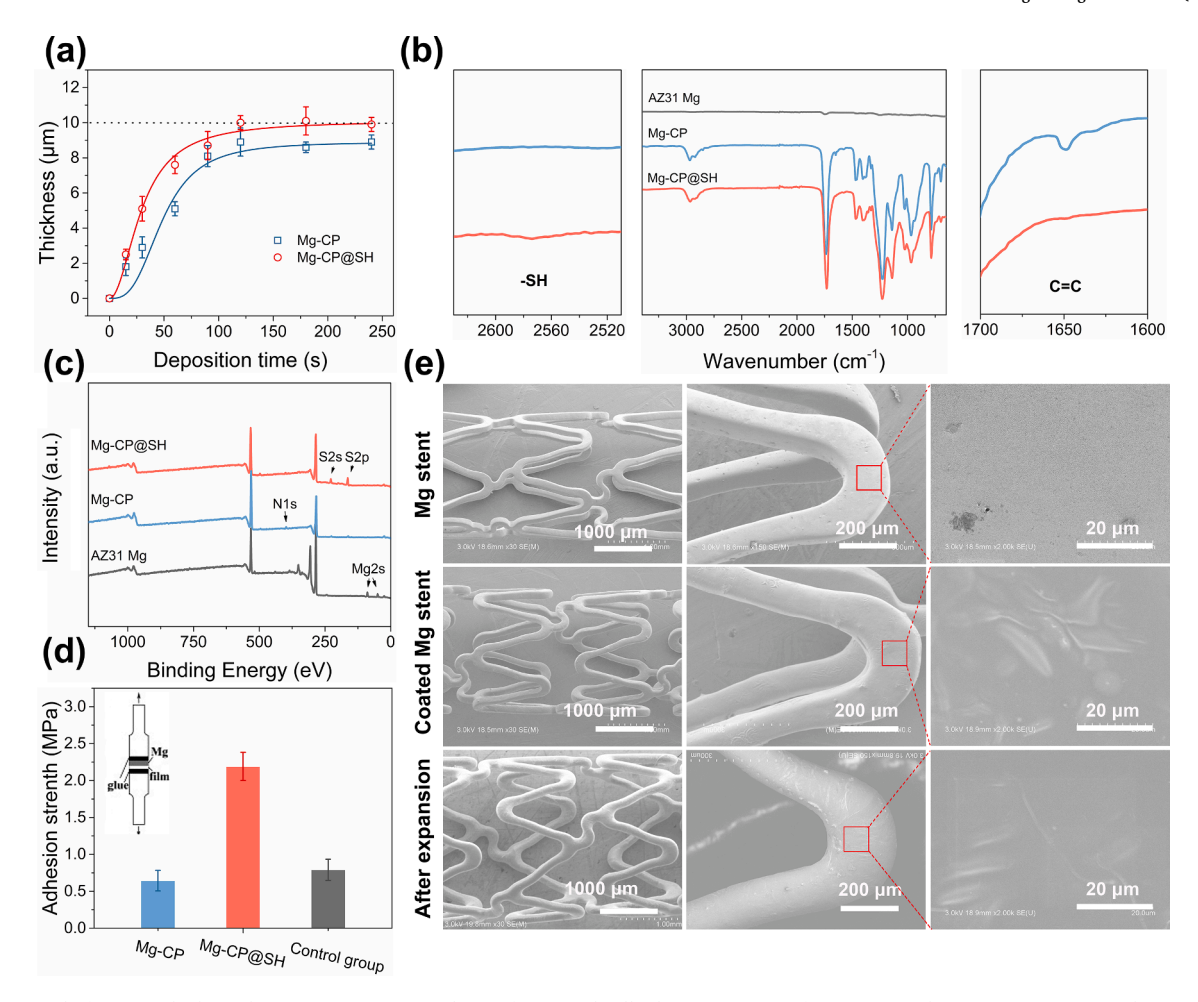


Fig. 1. (a) Control of coating thickness by EPD time (at EPD voltage of 40 V and colloid concentration of 15 mg/mL). (b) ATR-FTIR spectra and (c) XPS wide-scan spectra of AZ31 Mg and coated Mg samples. (d) Adhesion strength for different coated Mg samples, referenced to the standard of ISO 4624-2016. (e) SEM images of bare AZ31 Mg stent (top) and CP@SH-coated Mg stents before (middle) and after (bottom) expansion.

cm²) and bare Mg $(1.02 \times 10^3~\Omega~cm^2)$ (Fig. 2d). Thus, the Mg-CP@SH samples possessed excellent corrosion resistance, which conclusion could also be implied from the increased phase angles in Fig. 2e.

Equivalent circuits (ECs) proposed for fitting AZ31 Mg, Mg-CP, and Mg-CP@SH samples are shown in Fig. 2f, g, and h, respectively [47,48]. The corresponding data are listed in Table 1. In the EC model, R_s refers to solution resistance, which depends on the solution content; R_c denotes the resistance of corrosion product layer or coating, which also reflects their anti-penetrating ability for the electrolyte; R_{ct} is the charge transfer resistance which reflects the difficulty of redox reactions on the Mg interface. In addition, CPE1 and CPE2 are constant phase elements (CPEs) related to the double-layer capacitance; the decrease of CPE often indicates enhanced corrosion resistance. Finally, the induction L and induction resistance R_L describe the low-frequency inductive loop, representing the dissolution of Mg. The resistances R_c and R_{ct} increased due to the substitution of the loose corrosion product layer on bare Mg by the Mg-CP coating. R_c of Mg-CP@SH samples (3.41 imes 10⁵ Ω ·cm⁻²) sharply increased by two orders of magnitude compared with that of the Mg-CP sample (7.81 \times 10³ Ω cm⁻²), and *CPE*₁ also declined by a similar magnitude from 1.14×10^{-5} (Mg-CP) to 7.96×10^{-7} (Mg-CP@SH). These results implied that the enhanced corrosion resistance of CP@SH coatings was caused by the formation of thiol-ene networks enhancing the anti-penetrating ability. All coated samples possessed long-term stable corrosion resistance, and Mg-CP@SH samples kept their excellent corrosion resistance during the 144 h EIS test (Fig. S7).

2.3. In vitro long-term degradation tests

The long-term corrosive behaviors were investigated by an immersion test of 90 days in SBF (37 °C). The pH values and Mg²⁺ concentration of extracts of different samples were tracked (Fig. 3a and b) because both parameters relate to Mg corrosion. Bare Mg showed an extremely fast corrosion rate during the in vitro immersion test. Both pH value and Mg²⁺ concentration increased rapidly for bare Mg in the first 10 days. After that, the parameters increased at a lower rate and reached a maximum at 15 days due to the formation of a blocking layer of corrosion products, mainly Mg(OH)₂, on the surface of Mg alloy. The pH value (10) and Mg²⁺ concentration (~670 mg/L) remained stable after 15 days, probably due to the precipitation-dissolution equilibrium of Mg (OH) $_2$ [49]. Compared to bare Mg, the Mg-CP sample exhibited a slower change in pH and release of Mg $^{2+}$ representing a decreased corrosion rate of Mg substrate at the initial stage. This result indicated that Mg-CP coating slightly delayed the dissolution and pitting corrosion of Mg substrate in agreement with the conclusion obtained from EIS results. By contrast, the increase in both pH and ${\rm Mg}^{2+}$ concentration is much slower for the Mg-CP@SH sample, and, finally, values of about 8.5 and about 440 mg/L, respectively, were determined after 90 days of immersion, which implied that applying CP@SH coating with effective corrosion resistance endowed slow and relative uniform corrosion rate to Mg substrate. In addition, the weight loss of the Mg-CP@SH sample of 8.7% was much lower than that of Mg-CP (16.5%) and bare Mg (36.1%) (Fig. 3c). These findings indicated that Mg-CP@SH exhibited excellent anti-corrosion properties even in the rigorous 90-day immersion

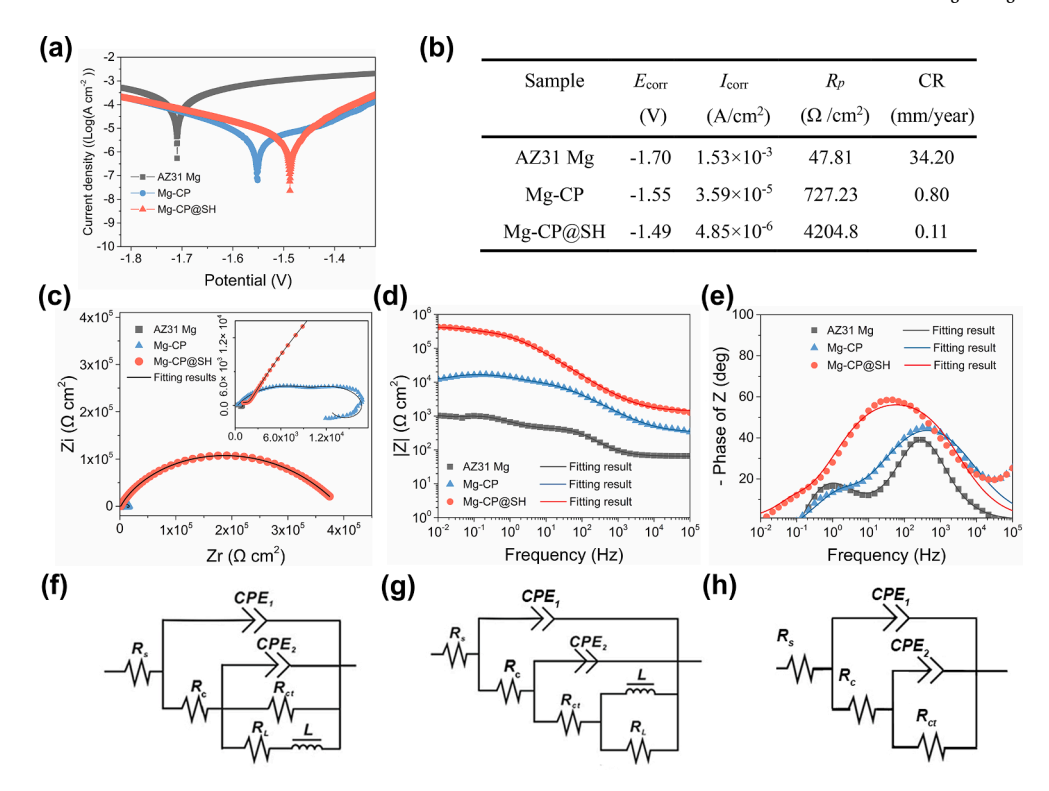


Fig. 2. Electrochemical corrosion test of AZ31 Mg, Mg-CP, and Mg-CP@SH samples in SBF (37 ± 0.5 °C) for 4 h. (a) Potentiodynamic polarization, (b) corrosion data analyzed from (a); (c) EIS Nyquist plots, (d) EIS Bode plots of |Z| vs. frequency, (e) Bode plots of phase angle vs. frequency; ECs of (f) bare Mg, (g) Mg-CP sample, and (h) Mg-CP@SH sample, data were fitted by ZSimpWin 3.4 software.

Table 1 EC parameters fitted from EIS plots.

Sample	R_s $(\Omega \cdot \text{cm}^2)$	CPE_1 ($\Omega^{-1}\cdot S^n\cdot cm^{-2}$)	n_1	CPE_2 $(\Omega^{-1}\cdot S^n\cdot cm^{-2})$	n_2	$R_{\rm c}$ $(\Omega \cdot {\rm cm}^2)$	$R_{\rm ct}$ $(\Omega \cdot {\rm cm}^2)$	$R_{\rm L}$ $(\Omega \cdot { m cm}^2)$	L (H·cm ⁻²)
AZ31 Mg	65.8	1.12×10^{-5}	0.85	6.74×10^{-4}	0.77	382.5	619.3	143	2.08×10^{-3}
Mg-CP	100.1	1.14×10^{-5}	0.38	3.68×10^{-6}	0.84	7.81×10^{3}	$1.13 imes 10^4$	7.48×10^{3}	3.54×10^{-4}
Mg-CP@SH	132.0	7.96×10^{-7}	0.69	4.21×10^{-5}	1	3.41×10^5	5.33×10^4	_	-

experiment.

The mechanism of long-term corrosion resistance of the Mg-CP@SH sample was intuitively revealed by SEM. The surface morphologies of different samples were examined before and after the immersion test (Fig. 3d). The bare Mg was severely corroded after 90 days, and its surface was fully covered with corrosion products. The coating on the Mg-CP sample revealed many hole defects due to inadequate adhesion and poor mechanical properties resulting in partial peeling of films and localized corrosion on the Mg substrate. In contrast, the Mg-CP@SH sample still appeared uniform, smooth, and with maintained surface integrity resembling that before immersion, suggesting that the coating protected the Mg substrate from aggressive SBF solution during the 90day test. The elements on the surface of three samples were detected after immersion tests by EDS (Fig. 3g). The corrosion products may be attributed to Mg(OH)2 that was found on AZ31 Mg and Mg-CP samples but was not observed on the Mg-CP@SH sample. Furthermore, as evident from the cross-section images of the Mg-CP@SH sample, the dense protective coating was continuously and firmly attached to the Mg surface (Fig. 3e), the change in thickness during the test confirmed the surface erosion behavior of CP@SH coating, and its degradation rate was estimated at about 1.9 µm per month. The corrosion that occurred underneath the transparent coating was first observed by an optical microscope (Fig. S8). In contrast to the severe corrosion of AZ31 Mg and pitting corrosion of Mg-CP, the only observed greyish corrosion products were evenly distributed under the CP@SH coating. To further examine

the corrosion degree of Mg substrates, their surface morphologies were observed by SEM after removal of the polymeric coating and corrosion products (Fig. 3f). Pitting holes (red arrow) like in the AZ31 Mg and Mg-CP samples were not present on the Mg-CP@SH sample, suggesting that the Mg substrate possessed homogeneous degradation behaviors due to the usage of CP@SH coating. In conclusion, the durable surface-eroding CP@SH coating inhibited the infiltration of corrosive media and the dissolution of corrosion product layer due to its good adhesion strength, which endowed the coating with outstanding long-term anti-corrosion performance and maintained mechanical properties of the Mg substrate. The uniform erosion rate of thiol-ene-crosslinked APC coatings may provide the possibility to regulate the corrosion rate of AZ31 Mg stents by adjusting the coating thickness, thereby adapting the degradation rate of AZ31 Mg stents with the repair process of surrounding vessel tissues.

2.4. Hemocompatibility test

The hemocompatibility of all samples was assessed by *in vitro* static adhesion assay and hemolysis test (Fig. 4). While few adherent platelets were visible on the AZ31 Mg surface (Fig. 4a), many deposited platelets with activation spread-dendritic morphologies [50] were observed on the PLGA-coated Mg sample which served as control group (Fig. 4d). In contrast, only a few round platelets without pseudopodia were present on the APC coatings (Fig. 4b, c). Thus, compared to the PLGA coating,

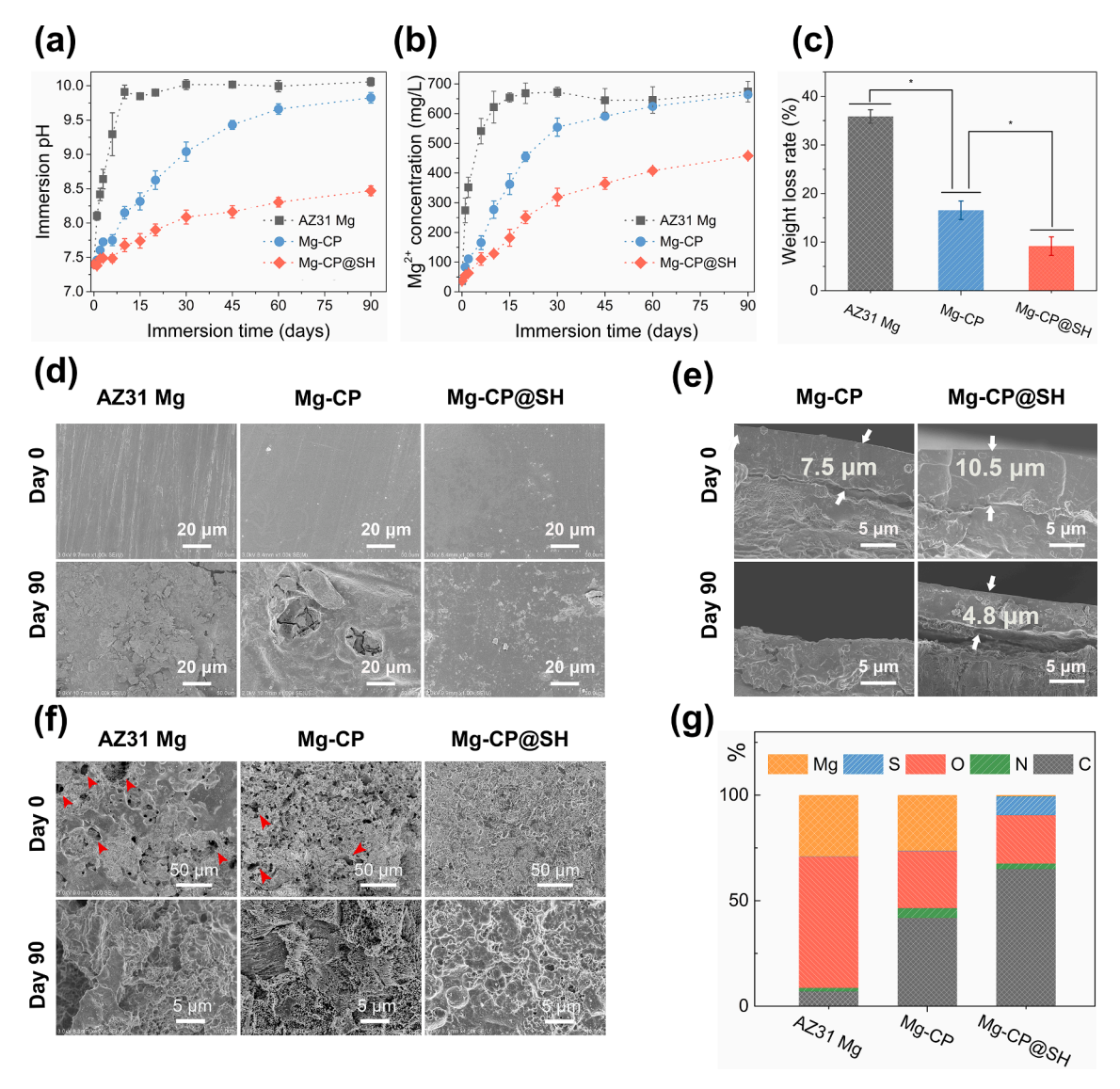


Fig. 3. Long-term degradation tests of bare Mg, Mg-CP, and Mg-CP@SH in vitro. (a) pH values, (b) Mg^{2+} concentration, and (c) the mass loss rate of the three samples in the 90-day immersion test in SBF; **p < 0.01. SEM images of (d) surface and (e) cross-section morphologies of all samples before and after 90 days of immersion. (f) SEM images of 90-day immersion samples after removal of the polymer coatings and corrosion products. (g) EDS results of samples after the 90-day immersion test.

the CP@SH coatings presented fewer and no activated platelets, which may reduce the probability of thrombus formation and arterial occlusion when applied on a Mg-alloy stent [51]. The results of the hemolysis test are shown in Fig. 4e. In general, a hemolysis rate of biomaterials below 5% is acceptable, whereas the rate of 17.48% of AZ31 Mg presented a significant hemolysis phenomenon. The low hemolysis rate of Mg-CP and Mg-CP@SH of 2.69% and 0.70%, respectively, could be attributed to the inhibition of excessive release of Mg $^{2+}$ and OH $^{-}$ by the APC coatings. Therefore, the CP@SH coating can reduce the risk of hemolysis for Mg implants. In summary, the thiol-ene-crosslinked APC coating benefited the hemocompatibility of AZ31 Mg.

2.5. In vitro cytocompatibility assay

The cell survival, adhesion, growth, and proliferation influence the endothelialization process of AZ31 Mg stents, which play essential roles in clinical application. Therefore, the adhesion and growth behaviors of endothelial cells on different samples were investigated. As shown in Fig. 5a, few live cells (green color) were present on AZ31 Mg after 24 h culturing, and almost only dead cells (red color) could be observed after

72 h culturing. The severe cytotoxicity was mitigated after coating modification. In contrast to AZ31 Mg, the number of dead cells declined on Mg-CP samples, while no dead cells were present on the Mg-CP@SH sample. Simultaneously, the number of live cells sharply increased after coating modification. In terms of cell morphology, the EA.hy926 cell on Mg substrate became round in shape without filopodia extensions, and cells presented in a deformed, shrunken, and irregular shape on the Mg-CP sample, implying that they weakly adhered to both bare Mg and Mg-CP samples. In contrast, EA.hy926 cells were fully stretched on the Mg-CP@SH surfaces, demonstrating their more superior cellular spreading and adhesion capability. Further quantitative results (Fig. 5b-c) showed that all coating samples benefited the growth of cells. Among them, the CP@SH coating provided a more ideal surface environment for endothelial cell adhesion, growth, and proliferation, which was confirmed by their largest numbers of living cells and coverage areas. This remarkable improvement of cytocompatibility seemed positively correlated to the corrosion resistance enhancement of the coatings. Thus, to verify this assumption, the cytotoxicity for extracts of all samples was assessed by MTT assay (Fig. 5d). Compared to the negative control group, the extract of AZ31 displayed obvious cytotoxicity with cell viability below 90%. In

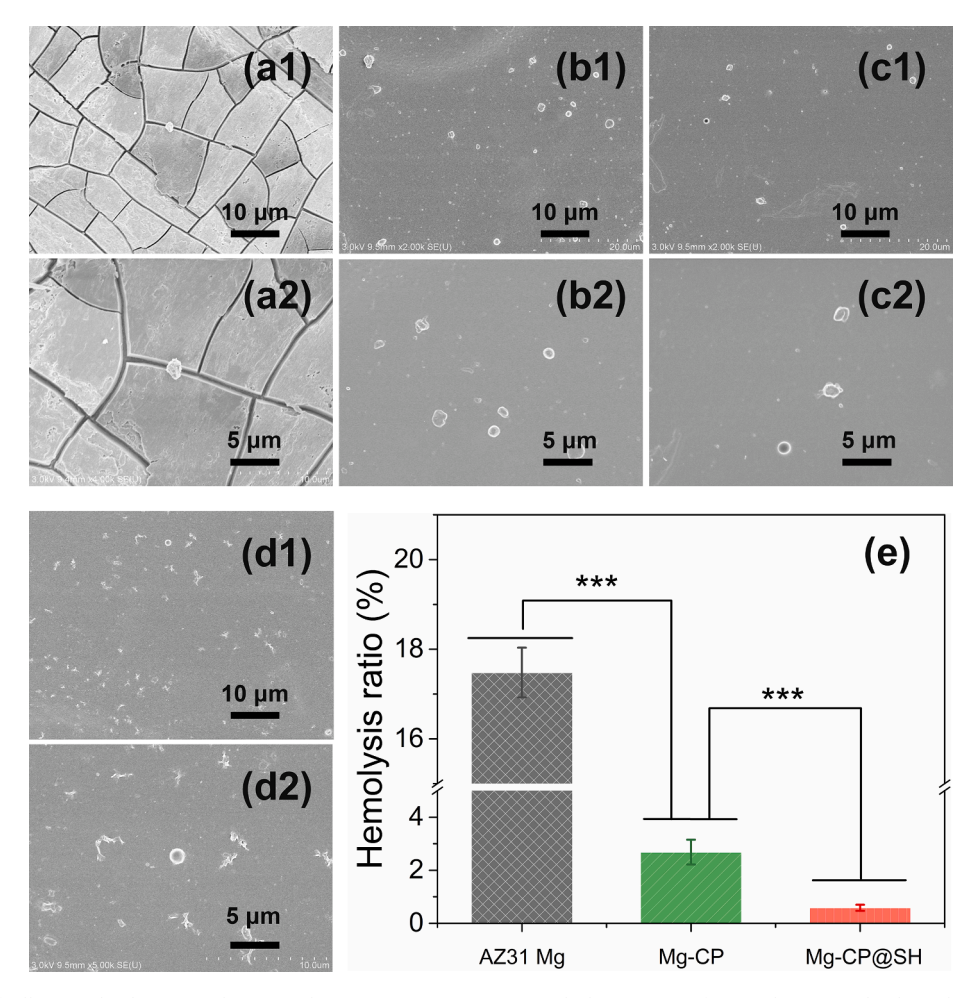


Fig. 4. Morphologies of adherent platelets on (a) bare Mg, (b) Mg-CP, (c) Mg-CP@SH, and (d) Mg-PLGA after incubation in platelet-rich plasma (PRP) observed by SEM. (e) The corresponding hemolysis rate of the three samples, ***p < 0.001.

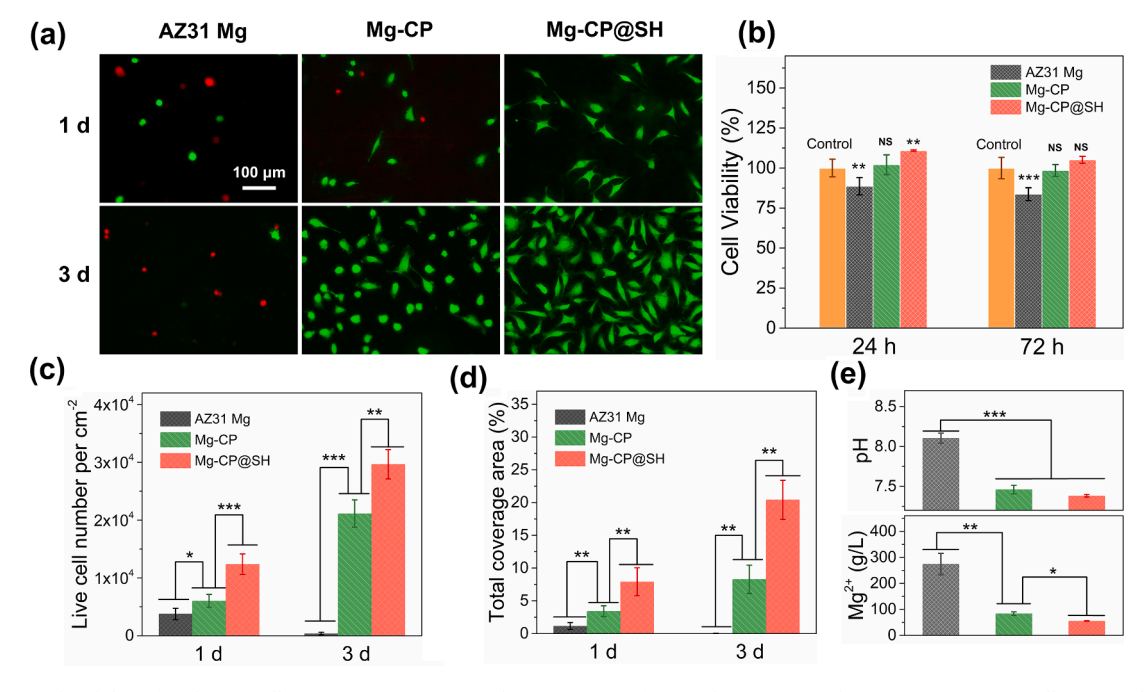


Fig. 5. Adhesion and viability of EA.hy926 cells on AZ31 Mg, Mg-CP, and Mg-CP@SH surfaces and extracts. (a) Fluorescence images of cells on samples stained with FDA (green) and PI (red) after incubation for 1 day and 3 days. (b) Cell viability of EA.hy926 incubated in 50% extracts of all samples for 1 day and 3 days (culture medium served as the extraction medium). Both (c) live cell numbers and (d) total coverage area analyzed from fluorescence images (each sample with at least 6 images). (e) The pH and Mg^{2+} concentration of extracts of all samples. * p < 0.05, ** p < 0.05, *** p < 0.001. (For interpretation of the references to color in this figure legend, the reader is referred to the web version of this article.)

contrast, the extracts of coated samples did not cause cytotoxicity. The measured pH value and ${\rm Mg}^{2+}$ concentration of extracts (Fig. 5e) indicated that the ${\rm Mg}^{2+}$ and ${\rm OH}^-$ ions released from Mg substrates led to the endothelial cell cytotoxicity. Based on these results, the thiol-enecrosslinked APC coatings provided a bioactive surface that improved the growth and proliferation of endothelial cells for Mg-alloy stents.

2.6. In vivo assessment

The rod samples of AZ31 Mg, Mg-CP@SH, and Mg-PLLA were prepared and implanted subcutaneously in Sprague-Dawley (SD) rats (Fig. 6a) to evaluate the *in vivo* corrosion resistance and tissue inflammation of CP@SH coating. The PLLA, a coating material widely used in drug-eluting stents, served as control group. For accurate visualization of the corrosion degree, micro-computed tomography (micro-CT) analysis was conducted. The 3D and 2D reconstruction images after 8-week implantation, shown in Fig. S9 (supporting information), revealed

obvious pitting corrosion on the AZ31 and Mg-PLLA samples; however, almost no corrosion occurred on the substrate of the Mg-CP@SH sample. After 16 weeks of implantation (Fig. 6b), the AZ31 and Mg-PLLA samples showed serious corrosion (white arrow), which was more severe than that of 8 weeks. In contrast, the Mg-CP@SH sample exhibited only negligible corrosion, which demonstrated the excellent in vivo corrosion resistance of CP@SH coating. Since the coating materials cannot be observed by X-ray spectroscopy, the degradation behavior of coatings was examined by SEM to investigate the correlation between coating degradation and Mg corrosion. After 8 weeks of in vivo degradation (Fig. S10), numerous deep cracks and pitting holes were present on AZ31 Mg. The coating on the Mg-PLLA sample was exfoliated from Mg on a large area, and the surface was veined with many corrosion cracks. By contrast, the CP@SH coating firmly adhered to the Mg substrate and presented surface erosion behavior, which inhibited the inhomogeneous pitting corrosion of Mg alloy. After 16 weeks of implantation (Fig. 6b), AZ31 showed a more severe corroded surface, losing shape integrity in

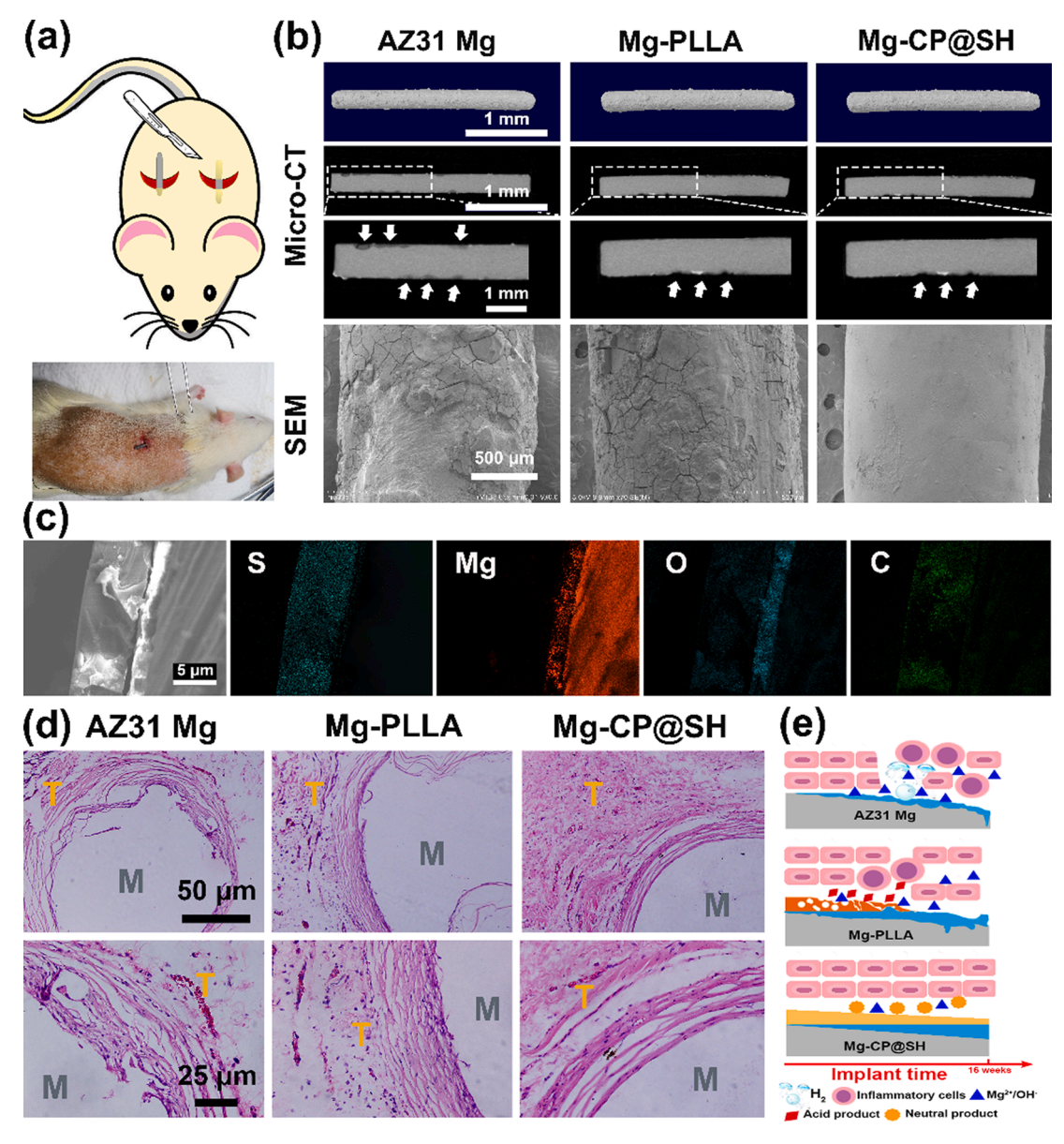


Fig. 6. (a) Schematic and digital photograph of the surgical process of subcutaneous implantation in SD rats. (b) 3D and 2D reconstruction micro-CT images and SEM images of AZ31 Mg, Mg-PLLA, and Mg-CP@SH rods at 16 weeks after subcutaneous implantation in SD rats; the PLLA coating serves as control group. (c) SEM images and elemental mapping (S, Mg, O, and C) of Mg-CP@SH 16 weeks after implantation. (d) Representative micrographs of histological H&E stained sections of the implants: AZ31 Mg, Mg-CP@SH, and Mg-PLLA; M area represents Mg rod; T area represents the tissue. (e) The proposed mechanism of corrosion resistance and tissue response during *in vivo* test for AZ31 Mg-, PLLA-, and CP@SH-coated Mg substrates.

the physiological environment. The Mg-PLLA sample started to exhibit corrosion pits on its surface, which may be attributed to the premature degradation and exfoliation of PLLA coating from the Mg substrate resulting in the quick loss of corrosion resistance. Fortunately, a relatively smooth and integer surface can be observed on the Mg-CP@SH sample, suggesting its superior corrosion resistance. The thickness of the CP@SH coating was monitored by SEM and showed linear erosion from initial about 8.8 µm at 8 weeks (Fig. S10) to about 6.1 µm at 16 weeks (Fig. 6c), which constituted a degradation rate of about 1.4 µm per month in vivo. The elemental mapping results for the cross-section of Mg-CP@SH after 16 weeks are shown in Fig. 6c. The CP@SH coating could be observed at the outermost layer, which can be confirmed by significant C and S enrichment. Subsequently, O and Mg enrichment was observed in the undercoat, which was attributed to the presence of a uniform corrosion product layer. Combined with the SEM results, degradation of Mg alloy occurred under the CP@SH coating. However, different from polyester PLLA coating, the excellent adhesion, good durability, and predictable surface erosion property of CP@SH coating resulted in the observed homogeneous and slow degradation behavior of Mg rods. The superior qualities of the CP@SH coating can be attributed to impeding the corrosion products from dissolving or peeling off the Mg substrate, which resulted in a uniform and relatively dense product layer above the residual Mg alloy that may further enhance the corrosion resistance of Mg implants.

Histological H&E staining was conducted to assess the tissue response of these implants after 16 weeks post-operation. Macroscopically, a few tiny gas bubbles were observed by the naked eye in the surrounding tissue of the AZ31 Mg rod, while there were neither any inflammation, necrosis nor discoloration present in the surrounding tissue of Mg-CP@SH and Mg-PLLA samples. From the microscopic assay in Fig. 6d, the tissue that tightly integrated with the implanted samples featured appreciable fibroblast proliferation in all samples. Severe inflammatory cell infiltration, many red blood cells, and few gas bubbles triggered by Mg corrosion were observed in the tissue around the AZ31 Mg alloy, whereas the PLLA-coated Mg rod showed a slighter inflammation response and fewer red blood cells. By comparison, Mg-CP@SH showed the lowest infiltration of inflammatory cells and few blood capillaries in their surrounding tissue, which may be attributed to their neutral as opposed to acidic degradation products.

In this work, pictorial models were proposed to try expanding on the in vivo degradation process (Fig. 6e). The rapid corrosion of AZ31 Mg resulted in the formation of H₂ gas bubbles and the release of toxic ions (Mg²⁺ and OH⁻), which could damage the surrounding cells and tissues, presenting obvious tissue inflammation. The pitting corrosion of Mg alloy would gradually become severe with increasing implantation time, which resulted in inhomogeneous degradation behavior and the premature loss of mechanical properties of Mg substrate. After the Mg substrate was modified by PLLA coating, the corrosion could be inhibited. However, as a polyester, PLLA presents bulk-erosion behavior, degrading from both interior and the exterior. Thus, the coating would be easily exfoliated from the substrate at the early stage of implantation, and its acidic degradation products may cause tissue inflammation [52]. According to some investigations, however, the acidic products might be neutralized by the released OH-, thereby reducing the tissue inflammation of the original Mg alloy [28]. This may explain why a slight inflammation response occurred on the Mg-PLLA sample. However, the inadequate corrosion resistance of PLLA may still lead to the inhomogeneous degradation of Mg at the mid-late stages of implantation. The CP@SH coating, a thiol-ene-crosslinked APC, demonstrated its potential application as coating materials for AZ31 Mg stents since it may maintain the mechanical integrity of the Mg stent after implantation. This behavior can be explained as follows: Firstly, the surface-eroding coating maintained surface integrity during in vivo implantation which prevented Mg from contacting physiological medium and ensured a homogenous degradation behavior of AZ31 Mg; secondly, CP@SH coating prevented the permeation of physiological

medium along the incompatible surface of polymer and substrate due to its outstanding adhesion and good durability; finally, the Mg-CP@SH sample showed an excellent tissue response, which might be attributed to the neutral degradation products and superior corrosion resistance of CP@SH coating. It is expected that Mg implants might degrade with a controllable rate along with the tissue repair process by regulating the thickness of thiol-ene-crosslinked APC coatings.

3. Conclusion

In conclusion, a photo-crosslinked aliphatic polycarbonate coating with predictable degradation behavior was designed and fabricated by the EPD method for enhancing the corrosion resistance and improving the surface biocompatibility of Mg-alloy stents. We proved that a uniform coating with controllable thickness can be prepared on AZ31 Mg stents due to the inherent superiority of EPD in comparison to other coating methods. The results of the balloon expansion test indicated excellent mechanical property and adhesion strength of the coating on AZ31 Mg stents. Significantly, the coating presented surface-erosion degradation behavior with a predictable constant erosion rate of 1.9 um per month and 1.4 um per month in vitro and in vivo, respectively. Our results indicated that the combination of photo-crosslinked PMDMT polycarbonate and EPD method provided the employed Mg alloy with excellent corrosion resistance, which could lead to slow and homogeneous degradation behavior of Mg-alloy stents. In addition, coating modification on Mg substrate resulted in reduced hemolysis rate, enhancement of the adhesion and proliferation of endothelial cells, and reduction in tissue inflammation. This versatile strategy presents a potential application to avoid premature loss of mechanical integrity and improve the surface bioactivity of Mg-alloy stents.

Declaration of Competing Interest

The authors declare that they have no known competing financial interests or personal relationships that could have appeared to influence the work reported in this paper.

Acknowledgements

This work was supported by the National Natural Science Foundation of China (51573073) and National First-Class Discipline Program of Light Industry Technology and Engineering (LITE2018-19).

Appendix A. Supplementary material

Supplementary data to this article can be found online at https://doi.org/10.1016/j.cej.2021.131596.

References

- [1] J. Fu, Y. Su, Y.X. Qin, Y.F. Zheng, Y. Wang, D. Zhu, Evolution of metallic cardiovascular stent materials: A comparative study among stainless steel, magnesium and zinc, Biomaterials 230 (2020), 119641.
- [2] M. Echeverry-Rendon, J.P. Allain, S.M. Robledo, F. Echeverria, M.C. Harmsen, Coatings for biodegradable magnesium-based supports for therapy of vascular disease: A general view, Mater. Sci. Eng. C. 102 (2019) 150–163.
- [3] S.J. Lee, H.H. Jo, K.S. Lim, D. Lim, S. Lee, J.H. Lee, W.D. Kim, M.H. Jeong, J.Y. Lim, I.K. Kwon, Y. Jung, J.K. Park, S.A. Park, Heparin coating on 3D printed poly (l-lactic acid) biodegradable cardiovascular stent via mild surface modification approach for coronary artery implantation. Chem. Eng. J. 378 (2019), 122116.
- approach for coronary artery implantation, Chem. Eng. J. 378 (2019), 122116.
 Z. Yang, X. Zhao, R. Hao, Q. Tu, X. Tian, Y. Xiao, K. Xiong, M. Wang, Y. Feng, N. Huang, G. Pan, Bioclickable and mussel adhesive peptide mimics for engineering vascular stent surfaces, Proc. Natl. Acad. Sci. USA 117 (28) (2020) 16127–16137.
- [5] M. Haude, R. Erbel, P. Erne, S. Verheye, H. Degen, D. Böse, P. Vermeersch, I. Wijnbergen, N. Weissman, F. Prati, R. Waksman, J. Koolen, Safety and performance of the drug-eluting absorbable metal scaffold (DREAMS) in patients with de-novo coronary lesions: 12 month results of the prospective, multicentre, first-in-man BIOSOLVE-I trial, The Lancet 381 (9869) (2013) 836–844.
- [6] T. Hu, C. Yang, S. Lin, Q. Yu, G. Wang, Biodegradable stents for coronary artery disease treatment: Recent advances and future perspectives, Mater. Sci. Eng. C. 91 (2018) 163–178.

- [7] L. Mao, L. Shen, J. Chen, Y. Wu, M. Kwak, Y. Lu, Q. Xue, J. Pei, L. Zhang, G. Yuan, R. Fan, J. Ge, W. Ding, Enhanced bioactivity of Mg-Nd-Zn-Zr alloy achieved with nanoscale mgf₂ surface for vascular stent application, ACS Appl. Mater. Inter. 7 (9) (2015) 5320–5330.
- [8] J. Li, L. Chen, X. Zhang, S. Guan, Enhancing biocompatibility and corrosion resistance of biodegradable Mg-Zn-Y-Nd alloy by preparing PDA/HA coating for potential application of cardiovascular biomaterials, Mater. Sci. Eng. C. 109 (2020), 110607.
- [9] F. Kiani, C. Wen, Y. Li, Prospects and strategies for magnesium alloys as biodegradable implants from crystalline to bulk metallic glasses and composites—A review, Acta Biomater. 103 (2020) 1–23.
- [10] J. Wang, L. Cui, Y. Ren, Y. Zou, J. Ma, C. Wang, Z. Zheng, X. Chen, R. Zeng, Y. Zheng, In vitro and in vivo biodegradation and biocompatibility of an MMT/BSA composite coating upon magnesium alloy AZ31, J. Mater. Sci. Technol. 47 (2020) 52-67
- [11] N.E.L. Saris, E. Mervaala, H. Karppanen, J.A. Khawaja, A. Lewenstam, Magnesium: An update on physiological, clinical and analytical aspects, Clin. Chim. Acta 294 (1) (2000) 1–26.
- [12] R. Radha, D. Sreekanth, Insight of magnesium alloys and composites for orthopedic implant applications – a review, J. Magnes. Alloy. 5 (3) (2017) 286–312.
- [13] H. Yang, X. Qu, W. Lin, D. Chen, D. Zhu, K. Dai, Y. Zheng, Enhanced Osseointegration of Zn-Mg Composites by Tuning the Release of Zn Ions with Sacrificial Mg-Rich Anode Design, ACS Biomater. Sci. Eng. 5 (2) (2019) 453–467.
- [14] S. Gaur, R.K. Singh Raman, A.S. Khanna, In vitro investigation of biodegradable polymeric coating for corrosion resistance of Mg-6Zn-Ca alloy in simulated body fluid, Mater. Sci. Eng. C. 42 (2014) 91–101.
- [15] C. Li, C. Yu, R. Zeng, B. Zhang, L. Cui, J. Wan, Y. Xia, In vitro corrosion resistance of a Ta₂O₅ nanofilm on MAO coated magnesium alloy AZ31 by atomic layer deposition, Bioact. Mater. 5 (1) (2020) 34–43.
- [16] Y.F. Zheng, X.N. Gu, F. Witte, Biodegradable metals, Mater. Sci. Eng. R Rep. 77 (2014) 1–34.
- [17] F. Gao, Y. Hu, G. Li, S. Liu, L. Quan, Z. Yang, Y. Wei, C. Pan, Layer-by-layer deposition of bioactive layers on magnesium alloy stent materials to improve corrosion resistance and biocompatibility, Bioact. Mater. 5 (3) (2020) 611–623.
- [18] P. Wang, J. Liu, S. Shen, Q. Li, X. Luo, P. Xiong, S. Gao, J. Yan, Y. Cheng, T. Xi, In vitro and in vivo studies on two-step alkali-fluoride-treated Mg-Zn-Y-Nd alloy for vascular stent application: enhancement in corrosion resistance and biocompatibility, ACS Biomater. Sci. Eng. 5 (7) (2019) 3279–3292.
- [19] C.Y. Li, L. Gao, X.L. Fan, R.C. Zeng, D.C. Chen, K.Q. Zhi, In vitro degradation and cytocompatibility of a low temperature in-situ grown self-healing Mg-Al LDH coating on MAO-coated magnesium alloy AZ31, Bioact. Mater. 5 (2) (2020) 364-376.
- [20] J. Zhang, H. Li, W. Wang, H. Huang, J. Pei, H. Qu, G. Yuan, Y. Li, The degradation and transport mechanism of a Mg-Nd-Zn-Zr stent in rabbit common carotid artery: A 20-month study. Acta. Biomater. 69 (2018) 372–384.
- [21] J. Liu, B. Zheng, P. Wang, X. Wang, B. Zhang, Q. Shi, T. Xi, M. Chen, S. Guan, Enhanced in vitro and in vivo performance of Mg–Zn–Y–Nd alloy achieved with aptes pretreatment for drug-eluting vascular stent application, ACS Appl. Mater. Inter. 8 (28) (2016) 17842–17858.
- [22] L.Y. Li, L.Y. Cui, R.C. Zeng, S.Q. Li, X.B. Chen, Y. Zheng, M.B. Kannan, Advances in functionalized polymer coatings on biodegradable magnesium alloys- A review, Acta. Biomater. 79 (2018) 23–36.
- [23] Z. Wang, Z. Sun, B. Han, Q. Zheng, S. Liu, B. Zhang, T. Duan, Biological behavior exploration of a paclitaxel-eluting poly-L-lactide-coated Mg-Zn-Y-Nd alloy intestinal stent in vivo, RSC Adv. 10 (26) (2020) 15079–15090.
- [24] M.H. Kang, K.H. Cheon, K.I. Jo, J.H. Ahn, H.E. Kim, H.D. Jung, T.S. Jang, An asymmetric surface coating strategy for improved corrosion resistance and vascular compatibility of magnesium alloy stents, Mater. Des. 196 (2020), 109182.
- [25] M. Haude, H. Ince, A. Abizaid, R. Toelg, P.A. Lemos, C. von Birgelen, E. H. Christiansen, W. Wijns, F.J. Neumann, C. Kaiser, E. Eeckhout, S.T. Lim, J. Escaned, H.M. Garcia-Garcia, R. Waksman, Safety and performance of the second-generation drug-eluting absorbable metal scaffold in patients with de-novo coronary artery lesions (BIOSOLVE-II): 6 month results of a prospective, multicentre, non-randomised, first-in-man trial, The Lancet 387 (10013) (2016) 31–39.
- [26] F. Von. Burkersroda, L. Schedl, A. Göpferich, Why degradable polymers undergo surface erosion or bulk erosion, Biomaterials 23 (21) (2002) 4221–4231.
- [27] N. Ostrowski, B. Lee, N. Enick, B. Carlson, S. Kunjukunju, A. Roy, P.N. Kumta, Corrosion protection and improved cytocompatibility of biodegradable polymeric layer-by-layer coatings on AZ31 magnesium alloys, Acta. Biomater. 9 (10) (2013) 8704–8713.
- [28] A. Srivastava, R. Ahuja, P. Bhati, S. Singh, P. Chauhan, P. Vashisth, A. Kumar, N. Bhatnagar, Fabrication and characterization of PLLA/Mg composite tube as the potential bioresorbable/biodegradable stent (BRS), Materialia 10 (2020), 100661.
- [29] Y. Li, S. Zhao, S. Li, Y. Ge, R. Wang, L. Zheng, J. Xu, M. Sun, Q. Jiang, Y. Zhang, H. Wei, Surface engineering of biodegradable magnesium alloys for enhanced orthopedic implants, Small 15 (51) (2019) 1904486.

- [30] Z. Hou, S. Chen, Z. Li, Z. Chen, J. Hu, J. Guo, P. Li, L. Yang, Controllable degradation of poly (trimethylene carbonate) via self-blending with different molecular weights, Polym. Degrad. Stab. 189 (2021), 109596.
- [31] Y. Chen, S.H. Ye, Y. Zhu, X. Gu, S. Higuchi, G. Wan, W.R. Wagner, Covalently-attached, surface-eroding polymer coatings on magnesium alloys for corrosion control and temporally varying support of cell adhesion, Adv. Mater. Interfaces. 7 (15) (2020) 2000356.
- [32] K. Pan, X. Li, L. Meng, L. Hong, W. Wei, X. Liu, Photo-Cross-Linked Polycarbonate Coating with Surface-Erosion Behavior for Corrosion Resistance and Cytocompatibility Enhancement of Magnesium Alloy, ACS Appl. Bio Mater. 3 (7) (2020) 4427–4435.
- [33] S. Bertlein, G. Brown, K.S. Lim, T. Jungst, T. Boeck, T. Blunk, J. Tessmar, G. J. Hooper, T.B.F. Woodfield, J. Groll, Thiol-ene clickable gelatin: a platform bioink for multiple 3d biofabrication technologies, Adv. Mater. 29 (44) (2017).
- [34] H. Qi, S. Heise, J. Zhou, K. Schuhladen, Y. Yang, N. Cui, R. Dong, S. Virtanen, Q. Chen, A.R. Boccaccini, T. Lu, Electrophoretic deposition of bioadaptive drug delivery coatings on magnesium alloy for bone repair, ACS Appl. Mater. Inter. 11 (8) (2019) 8625–8634.
- [35] S. Obregón, G. Amor, A. Vázquez, Electrophoretic deposition of photocatalytic materials, Adv. Colloid Interface Sci. 269 (2019) 236–255.
- [36] S. Hu, W. Li, H. Finklea, X. Liu, A review of electrophoretic deposition of metal oxides and its application in solid oxide fuel cells, Adv. Colloid Interface Sci. 276 (2020), 102102.
- [37] B.J.C. Thomas, A.R. Boccaccini, M.S.P. Shaffer, Multi-Walled Carbon Nanotube Coatings Using Electrophoretic Deposition (EPD), J. Am. Ceram. Soc. 88 (4) (2005) 980–982.
- [38] L. Besra, M. Liu, A review on fundamentals and applications of electrophoretic deposition (EPD), Prog. Mater. Sci. 52 (1) (2007) 1–61.
- [39] A.R. Boccaccini, S. Keim, R. Ma, Y. Li, I. Zhitomirsky, Electrophoretic deposition of biomaterials, J. R. Soc. Interface. 7 (suppl_5) (2010) S581–S613.
- [40] X. Cheng, D. Deng, L. Chen, J.A. Jansen, Sander.G.C. Leeuwenburgh, F. Yang, Electrodeposited assembly of additive-free silk fibroin coating from pre-assembled nanospheres for drug delivery, ACS Appl. Mater. Inter. 12 (10) (2020) 12018–12029.
- [41] C. Han, Y. Yao, X. Cheng, J. Luo, P. Luo, Q. Wang, F. Yang, Q. Wei, Z. Zhang, Electrophoretic deposition of gentamicin-loaded silk fibroin coatings on 3D-printed porous cobalt-chromium-molybdenum bone substitutes to prevent orthopedic implant infections, Biomacromolecules 18 (11) (2017) 3776–3787.
- [42] L.R. Rivera, A. Cochis, S. Biser, E. Canciani, S. Ferraris, L. Rimondini, A. R. Boccaccini, Antibacterial, pro-angiogenic and pro-osteointegrative zein-bioactive glass/copper based coatings for implantable stainless steel aimed at bone healing. Bioact. Mater. 6 (5) (2021) 1479–1490.
- [43] B. Wang, J. Hua, R. You, K. Yan, L. Ma, Electrochemically deposition of catecholchitosan hydrogel coating on coronary stent with robust copper ions immobilization capability and improved interfacial biological activity, Int. J. Biol. Macromol. 181 (2021) 435–443.
- [44] R. Sikkema, K. Baker, I. Zhitomirsky, Electrophoretic deposition of polymers and proteins for biomedical applications, Adv. Colloid Interface Sci. 284 (2020), 102272
- [45] C. Chen, J. Tan, W. Wu, L. Petrini, L. Zhang, Y. Shi, E. Cattarinuzzi, J. Pei, H. Huang, W. Ding, G. Yuan, F. Migliavacca, Modeling and experimental studies of coating delamination of biodegradable magnesium alloy cardiovascular stents, ACS Biomater, Sci. Eng. 4 (11) (2018) 3864–3873.
- [46] M. Golabadi, M. Aliofkhazraei, M. Toorani, A.S. Rouhaghdam, Evaluation of La containing PEO pretreatment on protective performance of epoxy coating on magnesium, Prog. Org. Coat. 105 (2017) 258–266.
- [47] Y.H. Zou, J. Wang, L.Y. Cui, R.C. Zeng, Q.Z. Wang, Q.X. Han, J. Qiu, X.B. Chen, D. C. Chen, S.K. Guan, Y.F. Zheng, Corrosion resistance and antibacterial activity of zinc-loaded montmorillonite coatings on biodegradable magnesium alloy AZ31, Acta Biomater. 98 (2019) 196–214.
- [48] J. Wang, Y. He, M.F. Maitz, B. Collins, K. Xiong, L. Guo, Y. Yun, G. Wan, N. Huang, A surface-eroding poly(1,3-trimethylene carbonate) coating for fully biodegradable magnesium-based stent applications: toward better biofunction, biodegradation and biocompatibility, Acta Biomater. 9 (10) (2013) 8678–8689.
- [49] M. Esmaily, J.E. Svensson, S. Fajardo, N. Birbilis, G.S. Frankel, S. Virtanen, R. Arrabal, S. Thomas, L.G. Johansson, Fundamentals and advances in magnesium alloy corrosion, Prog. Mater. Sci. 89 (2017) 92–193.
- [50] L.B. Koh, I. Rodriguez, S.S. Venkatraman, The effect of topography of polymer surfaces on platelet adhesion, Biomaterials 31 (7) (2010) 1533–1545.
- [51] X. Gu, Y. Zheng, Y. Cheng, S. Zhong, T. Xi, In vitro corrosion and biocompatibility of binary magnesium alloys, Biomaterials 30 (4) (2009) 484–498.
- [52] C.H. Kum, Y. Cho, Y.K. Joung, J. Choi, K. Park, S.H. Seo, Y.S. Park, D.J. Ahn, D. K. Han, Biodegradable poly(l-lactide) composites by oligolactide-grafted magnesium hydroxide for mechanical reinforcement and reduced inflammation, J. Mater. Chem. B. 1 (21) (2013) 2764–2772.